16th World Conference on Earthquake, 16WCEE 2017

Santiago Chile, January 9th to 13th 2017

Paper N° 4783

Registration Code: S-W1463279793

PHYSICAL MECHANISM AND PREVENTION METHOD OF LOESS SLOPE FAILURE INDUCED BY THE COUPLING EFFECT OF EARTHQUAKE AND RAINFALL

L. Wang[(1)], J. Sun[(2)], Q. Wang[(3)], X. Pu[(4)], N. Wang[(5)]

[(1)] *Professor, Lanzhou Institute of Seismology, China Earthquake Administration, Lanzhou 730000, China, wanglm2304@126.com*
[(2)] *Professor, Lanzhou Institute of Seismology, China Earthquake Administration, Lanzhou 730000, China, sunnjunj@163.com*
[(3)] *Assistant Professor, Key Laboratory of Loess Earthquake Engineering, China Earthquake Administration, Lanzhou 730000, China, wangq0930@126.com*
[(4)] *Associate Professor, Lanzhou Institute of Seismology, China Earthquake Administration, Lanzhou 730000, China, wdpuxw@163.com*
[(5)] *Postgraduate Student, Lanzhou Institute of Seismology, China Earthquake Administration, Lanzhou 730000, China, piaomiaolf2007@163.com*

Abstract

Earthquakes and rainfalls are the two most important factors to cause landslides. However, the coupling effect of the two factors on landslides is rarely considered in the slope stability analysis due to the lack of conclusive evidence of slope failure induced by the coupling effect. Unfortunately, some cases of massive failure of loess slopes and long distance sliding of mudflow caused by the Minxian-Zhangxian Ms6.6 Earthquake, Gansu Province, China in 2013 were seriously influenced by the persistent heavy rain before the earthquake. This should be the conclusive coupling event under earthquake and rainfall around the world. Those loess landslides induced by the Earthquake show the features associated with soil flow, among which the landslide at Yongguang Village, the largest one with more than 1.5km sliding distance, led to a serious loss of 14 households buried and 12 persons dead.

In this paper, firstly, the influence laws of water content on static and dynamic shear strength of loess soil were investigated by means of triaxial tests, dynamic triaxial tests and torsional shear tests. Secondly, the shaking table tests were performed with the three coupling patterns of earthquake and rainfall, i.e. a rainfall before and after an earthquake, and liquefaction triggered mud flow. In the tests, the time histories of acceleration, pore pressure and soil pressure in the loess slope model were recorded. Based on the tested results, the mechanism of failure and sliding of loess slopes induced by the coupling effect of earthquake and rainfall was analyzed. The critical PGAs causing gentle loess slope completely failure at different rainfall conditions were provided. And then, by means of the fuzzy information processing, the methods of predicting the sliding distance and the affected region of a landslide were presented respectively. Furthermore, a method of seismic safety design for the engineering practice to prevent the disaster of loess slope failures induced by coupling effect of earthquake and rainfall was proposed. The results shown that a rainfall may predominately decrease shear strength of loess deposit, which made loess slopes more easy to lose their stability under the effect of earthquakes due to an obvious decrease of static and dynamic cohesions and internal friction angles. The saturated loess layer in slopes may liquefy under the effect of strong earthquakes, which usually trigger a long distance soil flow. Earthquakes may cause some fissures in the vertical direction in loess deposit, which may favor the down seepage of rainfall in the loess slopes. Therefore, a persistent rainfall or heavy rainfall after an earthquake may easily induce landslides in loess areas. For the above-mentioned reason, the coupling effect of earthquakes and rainfalls on stability of loess slopes should be well considered in landslides disaster mitigation and risk management of landslides.

Keywords: loess slope, failure, coupling effect, earthquake, rainfall

1. Introduction

Landslide is a widespread hazard as well as a major geomorphic process affecting landscape evolution in mountainous regions around the world[1]. The hazard causes not only considerable financial losses but also major ecological and environmental problems[2]. Each year landslides cause more than 100,000 deaths and injuries, with damage costing more than 1 billion USD[3]. In many countries, the economic losses and casualties caused by landslides are greater than commonly recognized, and this kind of disaster generates a yearly loss of property larger than that from any other natural disaster including earthquakes, floods and windstorms[4].

Loess is a kind of collapsible soil with weak cohesion and porous microstructure formed in Quaternary. It is widely distributed in the Loess Plateau of China with an area of 440,000km^2 and a thickness of tens meters to hundreds meters, where is also seismically active region with three major seismic belts and were affected by more than 96 strong and great earthquakes with a magnitude of Ms$\geqslant$6.0 in history. Both earthquakes and rainfalls induced a lot of landslides in the loess area, which caused a huge casualties and economic loss. However the coupling effect of earthquakes and rainfalls on loess landslides has been not studied until such an effect appeared in the field investigation of the Minxian-Zhangxian Ms6.6 earthquake of China in 2013[12]. Before the earthquake, there was persistent raining for several days in loessial mountainous area. The water content increased in loess slopes, which decreased the dynamic shear strength of loess deposit. Under the effect of the earthquake, many landslides were induced within an area of 30km long and 8km wide affected by the earthquake with the intensity of VII and VIII degree. The largest one is a liquefaction-triggered mudflow in a loess slope with an average gredient of 18^o at Yongguang vallige, which slided forward for about 1km with a loess mass of 400,000 m^3 and formed a backwall of 100m wide and 30m high. In this paper, the physical mechanism and prevention method of loess slope failure induced by the coupling effect of earthquakes and rainfalls were studied based on the field tests, shaking table tests and dynamic torsional tests.

2. Influence of Water Content on Loess Strength

Loess landslides usually develop in the wind-laid loess deposit formed in the late Pleistocene period of Quaternary (Q_3), called Malan loess. In order to investigate the influnce of water content on static and dynamic shear strength of loess, CU traxial tests, dynamic triaxial tests and torsional tests were performed on undisturbed loess specimens taken from a site in Lanzhou, Gansu province of China. All of the samples are Malan loess deposited during Quaternary period (Q_3). Their physical parameters are shown in Table 1.

Table 1 – Physical properties of loess specimens

Depth (m)	ρ (g/cm^3)	ρ_d (g/cm^3)	ω (%)	PL (%)	PI	Grain composition (%)		
						Clay (<0.005mm)	Silt (0.005~0.075mm)	Sand (>0.075mm)
5	1.34	1.28	5.04	17.2	7.3	14.5	68.2	17.3
10	1.36	1.30	4.25	18.5	7.5	17.1	66.5	16.4

The test apparatus is WF-12440 HCA made by Wykeham Farrance Ltd.in the UK with a saturated system of back pressure, i.e. a gas-water system controlling the saturation rate. In the static CU triaxial tests, loess specimens were processed as cylinders with 50mm in diameter and 100mm in height. Cell pressure σ_3 were respectively taken as 50kPa, 100kPa and 150kPa. And then, specimens were sheared with a deformation rate of 0.6mm/min until the principal stress difference (σ_1-σ_3) reached to a maximum value, after which it decreased with the strain increase, or the axial strain reached to 15%. The effective shear strength parameters, c' and φ', are calculated by Mohr's cycle and strength envelope based on Mohr-Coulomb theory (Fig. 1).

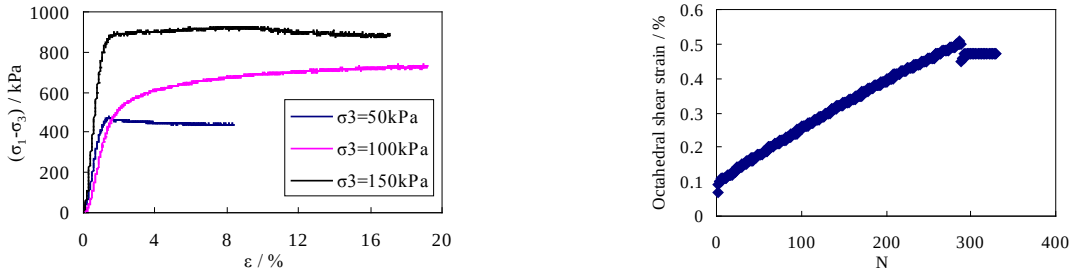

Fig. 1 – Relationships of principal stress difference versus strain (left), and octahedral shear strain versus cyclic times (right), for undisturbed specimens with burial depth of 5m

Loess specimens for dynamic triaxial tests were the same in size and shape as those in the above static testing. But for dynamic hollow cylinder torsional shear tests, the specimens were processed as hollow cylinders with 100mm in diameter outside, 60mm in diameter inside and 200mm high. All of specimens were respectively suffered an isotropic consolidation with cell pressure σ_3 of 100kPa, 150kPa and 200kPa. Dynamic loading was equiamplitude sinusoidal wave with a frequency of 1Hz and three different amplitudes, which can ensure the cyclic times of failure are little than 10, 10 to 20 and dozens respectively. The axial strain, ε_d, of 3% was adopted as the standard of loess specimen failure (Fig. 1).

Based on the results of static triaxial tests, static strength parameters including cohesion and angle of internal friction under different water contents are figured out (Fig. 2). The results indicate that water content has an obvious impact on dynamic strength of loess. Both cohesion and angle of internal friction decrease with the increase of water content. The former showes a nonlinear developing process and the latter follows nearly linear relatioship. Cohesion reduced rapidly with the increase of water content in a range lower than 15%, and then the curve becomes gentle. While the water content increases, soluble salts which play roles in cementation in the loess microstructure are dissolved in water, which will reduce cohesion among particles and cause the soil structure strength to decrease significantly, and finally it trends to be stabilized. However, the angle of internal friction mainly reflects the meshing effect among soil particles, which will decrease linearly with increasing of water contents of loess due to the soften effect and rearrangement of particles.

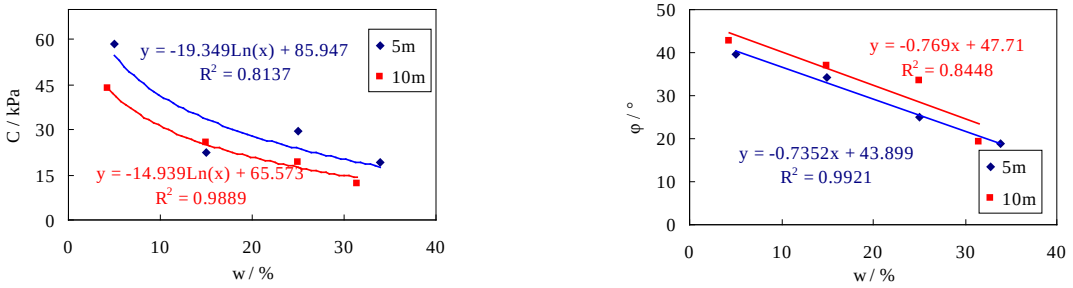

Fig. 2 – Relationships of cohesion (left) and angle of internal friction (right) respectively versus water content

In order to investigate the influence of water content on dynamic strength, both dynamic torsional shear tests and dynamic traxial tests were performed. To simulate the earthquake intensities of VII and VIII degree, sinusoidal loadings with cyclic times of 10 and 20 and 1Hz frenquency were employed in the dynamic tests. Dynamic strength parameters including dynamic cohesion and dynamic angle of internal friction of loess specimens with different water contents were calculated based on the test results. The relationships between dynamic strength parameters and water content are shown in Fig. 3. The results indicate that dynamic strength parameters, C_d and φ_d, decrease with increase of water content, w. The curves of C_d-w and φ_d-w with cyclic times of 10 and 20 show similar laws with those of the above-mentioned static strength versus water content. That is, C_d will decrease significantly when water content is lower than plastic limit of the loess, while the curves will become gentle when water content is higher than its plastic limit. However, the decrease of φ_d with

the increase of w is in a small range, which shows C_d is a more important factor to contribute decline of dynamic strength of loess with increase of water content. Of course, relationships between C_d and w also can be fitted as logarithmic function, while φ_d and w have a significant negative linear relationship under different cyclic times.

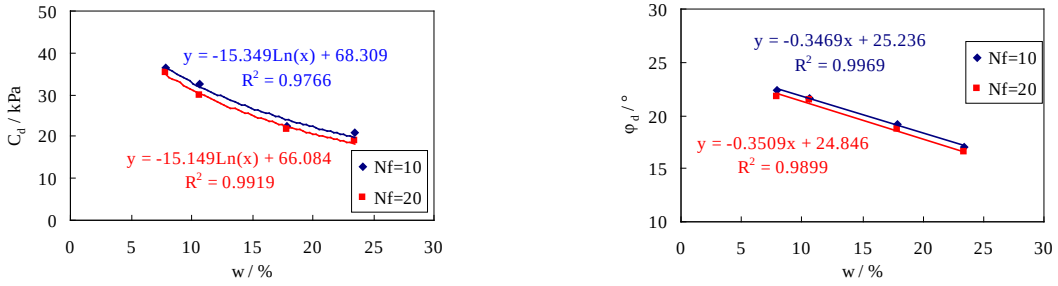

Fig. 3 – Relationships of dynamic cohesion (left) and angle of internal friction (right) versus water content with cyclic times of 10 and 20.

3. The Mechanism of Slope Failure

3.1 Loess slope model and dynamic loadings

Shaking table tests were performed to investigate the mechanism of loess slope failure under the coupling effect of earthquake and rainfall. The shaking table used in the tests may vibrate in horizontal and vertical directions with the maximum acceleration of 1.7g and a frequency range of 0.2-50Hz, which are 6m long and 4m wide. A real Malan loess（Q_3）slope with a height of 7m and a gradient of 20° were simulated by a tested model on the shaking table. The tested model and the layout of sensors of measuring acceleration, pore pressure and soil pressure in the model are shown as Fig.4, which is 2820mm long in the bottom, 1000mm high, 1400mm wide and 20° gradient in a certain similarity with the real slope. The model material was mainly selected as remolded loess to satisfy conditions of similar physical properties such as cohesion, internal friction angle and other parameters relying on controlling density and water content of remolded loess shown in Table 2. Sinusoidal waves with different frequencies of 3-50Hz and the EW component of ground acceleration of the Minxian Ms6.6 Earthquake in 2013 with a peak acceleration of 231gal and a predominant frequency of 4.2Hz recorded in Minxian county were employed as dynamic loadings (Fig. 5). The loading conditions are presented in Table 3.

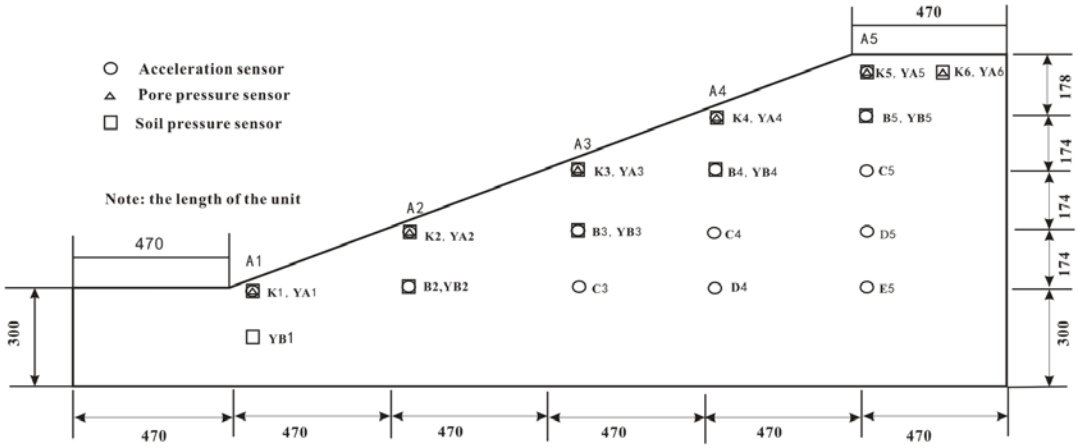

Fig.4 The tested slope model and the sensors layout

Table 2 - The soil parameters of shaking table model

Parameters	Similar constant	Actual value	Target value	Measured value
Cohesion (kPa)	10	43.2～50.2	5	9
Density (10^3kg/m^3)	1	1.31～1.34	1.32	1.32
Internal friction angel (°)	1	35～37	36	33

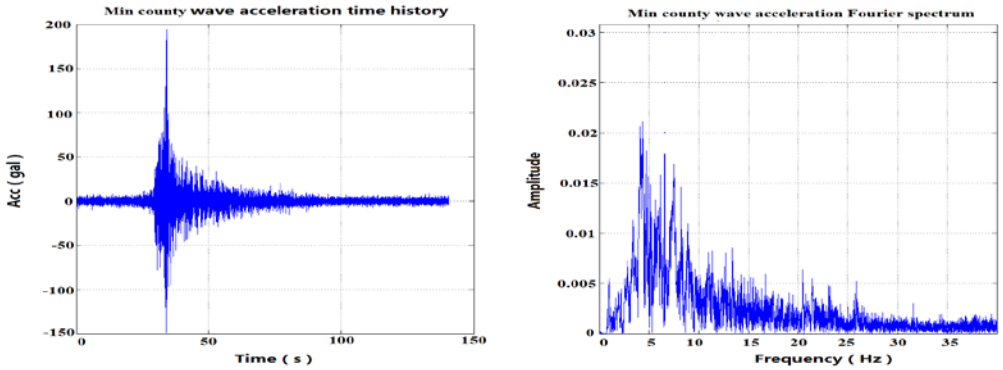

Fig. 5 – The time history and spectrum of Minxian Ms6.6 earthquake ground motion

Table 3 - Loading conditions

Serial number	Intensity	Input wave	Peak acceleration	Direction
1	VI (0.05g)	Sine wave（constant amplitude, 3～50Hz）	50gal	Horizontal
2	VII (0.1g)	The original/compressional Minxian wave	100gal	Horizontal
3	VIII (0.2g)	The original/compressional Minxian wave	200gal	Horizontal
4	IX (0.4g)	The original/compressional Minxian wave	400gal	Horizontal
5	IX (0.6g)	The original/compressional Minxian wave	600gal	Horizontal
6	X (0.7g)	The original/compressional Minxian wave	700gal	Horizontal
7	XI (1g)	The original/compressional Minxian wave	1000gal	Horizontal

3.2 Testing case of 10mm rainfall

(1) Failure characteristics

After 10mm rainfall, the saturation of slope surface soil in the range of 5mm reaches 30%-50%. Under the effect of dynamic loadings of 100gal and 200gal, there was no failure in the slope model, neither seismic subsidence nor vertical fissure to develop. When the loading exceeded 400gal, several obvious extensional fissures appeared, especially in slope shoulder where the fissure is 3mm to 5mm wide, and obvious X fissures appeared

in the upper part of slope surface. As the loading increased larger than 700gal， open fissures developed from slope top to its upper part with the depth of 60cm. And the slope failure was induced by a sliding of 2cm at the middle part of the slope, seismic subsidence of 2cm at the slope top and tensional fissures (Fig. 6 right).

Under the dynamic loading of 1000gal, slope model was damaged seriously and large fissures spread all over the upper part of the model and the biggest one reached 5cm wide. Soil mass in a certain range of the upper slope slid with the maximum value of 5cm. Seismic subsidence developed obviously near the slope shoulder with the maximum value of 5cm and gradually decreased from the top to bottom (Fig.6 left).

Fig. 6 – Failure of the slope model with 10mm rainfall in the shaking table tests (left:1000gal; right: 700 gal)

(2) Pore pressure within the model

Six pore pressure sensors, K1 ~ K6, were laid from the toe to the top of the slope model. When the loading was 100 and 200gal, there was no obvious change of the pressure. As the loading increased greater than 400gal, Obvious negative pore pressure change at many parts of slope from the bottom to the shoulder appeared. Under the loading of 700gal, pore pressure at each point varied alternately from positive value to negative value. Under the loading of 1000gal, a negative change with the biggest value of -0.65kPa appeared at K6 point with a long duration (Fig. 7), and a few big tensile fissures developed in the same part.

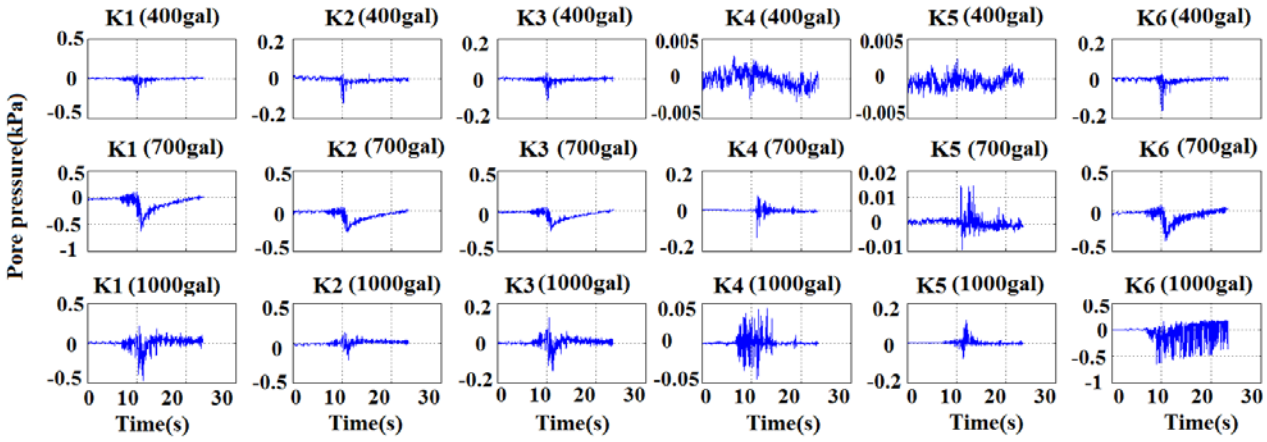

Fig. 7 – Variation of pore pressure of the slope model in the case of 10mm rainfall

3.3 Testing case of 100mm rainfall

(1) Dynamic loading of 600gal

After 100mm rainfall, penetrating front at the slope top and bottom is about 30cm deep under the slope surface, and the water content of soil in the front part ranges from 64% to 73%; The water content of soil near the slope

surface ranges from 56% to 68%. A few fissures were caused by collapse of loess before the test (Fig.8 left). Under the dynamic loadings of 100gal and 200gal, the model hardly had any change. Under the loading of 300gal, there was a little water to come out in three locations on the surface. In the case of 400gal loading, the displacement mark point in the slope shoulder slid about 3cm, and there was some water to come out from this point. Consequently, seismic subsidence was caused from 1cm to 2cm in this region (Fig.8 right). The fissures developed further.

Fig. 8 – Failures of the slope model with 100mm rainfall (left) and then under the loading of 400gal (right)

When the loading was 600gal, obvious liquefaction occurred on the slope top. The upper part of the slope slid down for 9cm and settled for 5cm (Fig.9 left). The pore pressures at K2, K3, K4 and K5 developed rapidly and then kept in a high value (Fig.10). The increase at the point K2 was about 2.8kPa, which is much higher than the overburden pressure of 0.8kPa at the same point. The pore pressure at the point K3 raised rapidly to the largest value of 0.8kPa, closing the overburden pressure, and then decrease slowly after loading. The pore pressures at the point K4 and K5 increased to 0.1kPa and 0.55kPa respectively. Both the failure phenomena of the slope model and rapid increase of the measured pore pressures indicated that liquefaction was induced by the coupling effect of shaking and rainfall.

(2) Dynamic loading of 650gal

Under the loading of 650gal, liquefaction triggered mudflow at the upper part and the bottom of the slope. The loess mass slid down for 20cm and formed the step-shape top and tensional fissures on the upper and middle part of the slope (Fig.9 right). The pore pressures at the point K1, K4 and K5 raised to 1.5kPa, 0.15kPa and 0.7kPa respectively, which made water to come out from the bottom of the slope. However, the pore pressure at the point K2 and K3 developed respectively from negative value to positive value and from positive value to negative value, which might be caused the complicated effects of sliding, traction, extruding, tension and settlement of the slope soil. The different pore pressures of 0.37kPa, 0.55kPa and 0.65kPa at the point K5 corresponding to the loadings of 400gal, 600gal and 650gal respectively also indicated that the slope soil liquefied in different extents under the loadings of different intensities (Fig. 10).

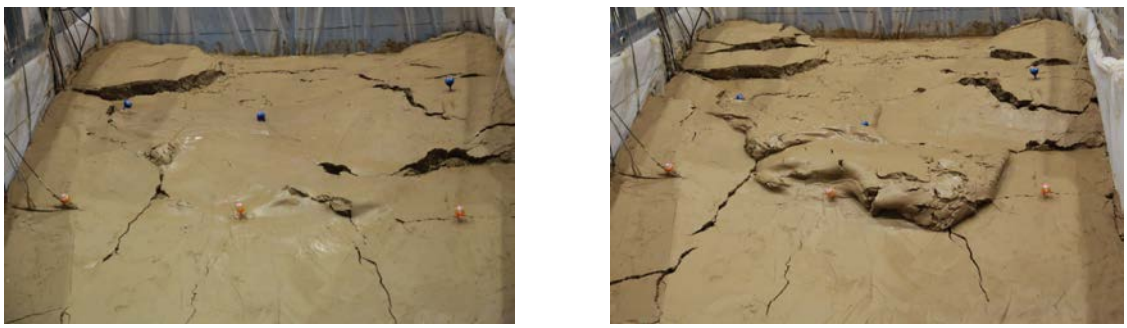

Fig. 9 – Failure of the slope model with 100mm rainfall induced by liquefaction (left: 600gal; right: 650 gal)

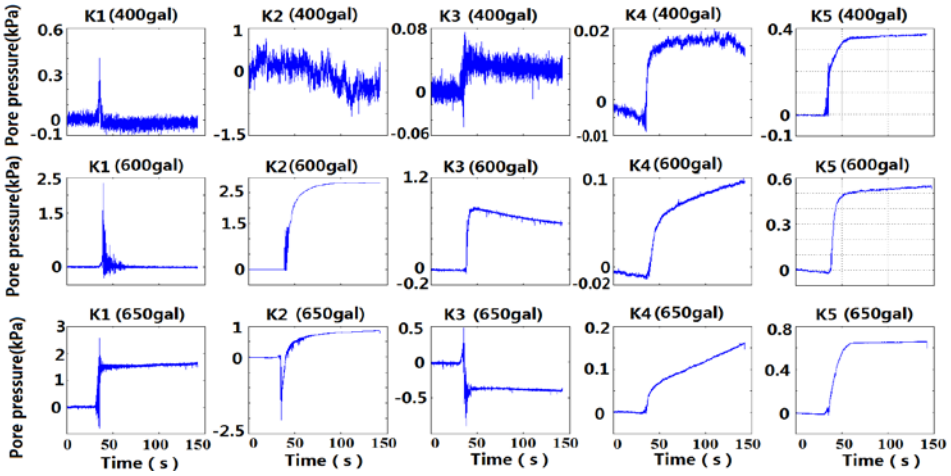

Fig. 10 – Variation of pore pressure in the loess slope in the shaking table tests.

3.4 Slope failure mechanism under the coupling effect

Based on the above-mentioned shaking table tests, the relationship between the critical PGA to cause a gentle loess slope completely failure and rainfall is obtained shown in Fig.11. It shows that the critical PGA decreases obviously with increase of rainfall, which could be very high, up to 1000gal, without rainfall and go down dramatically to 600gals with 100mm rainfall. With different rainfalls of lower than 5mm, 5-55mm and 55-100mm, the main cause of the loess slope failure is respectively crack, seismic subsidence and liquefaction under the effect of earthquake, which made both the soil mass damage and the slope lose its stability to slide.

A normal rainfall influences the stability of loess slope without vertical fissures only in a limit extent, because such a rainfall could not enter the deep soil of the slope. In this case, a middle-strong earthquake hardly causes the slope to lose its stability and slide, even if the top part of the slope may develop a little seismic subsidence and some fissures. In a case of heavy rainfall before an earthquake, the water content will increase in certain range of slope soil, even local soil mass is saturated. Consequently, the dynamic strength of wetted or saturated soil will decrease predominantly. And then an earthquake occurs, the increase of pore pressure would reduce the strength of soil further. The loess slope would easily lose its stability and slide. In addition, soil subsidence or liquefaction may increase the mobility of soil mass, which may trigger landslides and mudflow. In the case of liquefaction, mudflow would move down for a long distance, which could bury houses, destroy farmlands and roads, and even induce other disasters by its huge kinetic energy.

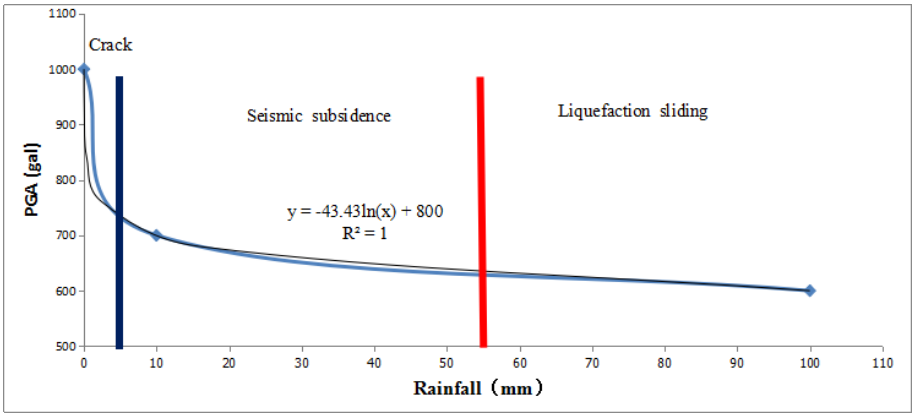

Fig. 11 – The critical PGA causing loess slope completely failure at different rainfall conditions

4. The Method of Predicting Sliding Distance

4.1 Definition and method

There are many definitions of sliding distance for landslide proposed by different researchers. In this paper， the sliding distanceof landslide, L, is defined as the distance from the back wall where the highest original part of the sliding body to the farthest place (Fig. 12). In the figure, the dashed curve is the original surface of a slope and the solid curve denotes the surface of the slope after sliding, including the parts of the back wall, sliding bed and the surface of sliding soil mass. Meanwhile, a method of fuzzy information processing (FIP) was applied to predict the sliding distance. The theory of FIP is shown as follows.

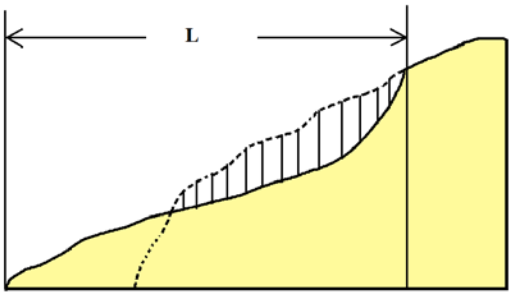

Fig. 12 –The sliding distance of a landslide

Assuming that X is an independent variable field or causes field, and Y is an dependent variable field or results field, one field is always expressed by a finite number of discrete points in a practical approximateresoning model as follows.

$$X=\{x_1,x_2,\ldots,x_n\} \quad (1)$$

$$Y=\{y_1,y_2,\ldots,y_n\} \quad (2)$$

If A_0 belongs to an observing event, X_0 is the cause and Y_0 is the result, then A_0 can be expressed as $A_0(x_0,y_0\}$, namely that $A_0=A_0(x_0,y_0\}$. If R is used to describe the observing event A, in order to establish causality between cause X and result Y. And then R can be expressed as follows.

$$R=R(A) \quad (3)$$

Therefore, when the cause X_0 is known, Y_0 can be inferred by rational approximate inference rules "|" as follows.

$$Y0=X0|R0 \quad (4)$$

4.2 Calculation procedure

The three indexes gradient, relative altitude of a slope and earthquake intensity were selected to calculate the sliding distance of earthquake-induced landslides by using fuzzy information optimization processing method. Calculation procedures include information distribution, information diffusion, information integration and the error checking.

After obtaining certain samples of knowledge, establishing fuzzy relation matrix relying on information distribution can make less samples distribute and dispose information. One dimensional information distribution formula is used to distribute varieties of parameters information to get cause set X in this paper.

Two-dimensional normal information diffusion equation is used to establish fuzzy relation matrix and diffuse information to obtain the original information distribution matrix. Then, the fuzzy relation matrix can be got by disposing original information distribution matrix normally.

Approximate reasoning results is used to analyze deduction sets by information centralized method, then final results have been obtained. The formula of information centralized method is as follows.

$$Y = \sum_{r=1}^{n} \mu^{k}(y_r)_i / \sum_{r=1}^{n} \mu^{k}(y_r) \tag{5}$$

In this formula, Y is final results of deduction, y_r is the grade value which still needed to be deducted, $\mu(y_r)$ stands for the membership values of approximate deduction result elements in the model.

4.3 Practical case

The sliding distance of loess landslides induced by an earthquake obtained from fuzzy information processing will be compared by the results calculated by other methods such as empirical statistical formula (ESF), Scheidegger's formula (SF), Moriwaki formula (MF), and empirical formula (EF). Depending on the comparison of standard deviation results from five models, the precision of fuzzy information optimization processing methods could be sure for loess landslides.

The Tongwei earthquake was taken as an example. On June 19,1718, a strong earthquake with a magnitude of 7.5 on the Richter scale occured in Tongwei county, Gansu province, China. The geographic coordinates of epicenter is 35.08°N and 105.20°E. The earthquake intensity in the meizoseismal region is X degree. Many large loess landslides were caused by this earthquake shown in Table 4.

Table 4 – Landslides induced by the Tongwei earthquake in China

Number	Toponym	Relative altitude (m)	Sliding distance (m)	Volume (m^3)	gradient
1	Yangjiasi western	185	400	24	18°
2	Shuixing town western	70	150	2.8	25°
3	Shuixing town western	110	450	12	20°
4	Wangjiazhuang	100	270	2.5	28°
5	Yejiapo	85	470	2.3	28°
6	Anyuan town western	180	1000	38	23°
7	Anyuan town northern	90	370	2.5	18°
8	Changjiahe Eastern	120	340	2.7	26°
9	Sanping	170	770	28	16°
10	Gaojiadian	190	840	54	17°
11	Gujiping	170	1250	185	11°
12	Dahecha	210	890	78	47°
13	Shuangmiao	170	550	17	19
14	Hongyan	240	780	120	42°
15	Yaojiagou	160	650	41	24°

In Table 4, 95 percent sliding distance, L, ranges from 150 to 1250 meters, and the relative altitude, H, is from 70 to 240 meters. The average gradient ranges from 11°to 47°, and the intensity is from VII to IX. By means of FIP, the field of each parameter is as follows.

$$V_L=\{L_1, L_2, L_3 \ldots L_8\}=\{150,300,450,600,750,900,1050,1200\}; \quad (6)$$

$$\mu_H=\{H_1,H_2,H_3 \ldots H_8\}=\{70,90,110,130,150,170,190,210\}; \quad (7)$$

$$\mu_\alpha=\{\alpha_1,\alpha_2,\alpha_3 \ldots \alpha_7\}=\{11,17,23,29,35,41,47\}; \quad (8)$$

$$\mu_M=\{M_1, \quad M_2, \quad M_3 \quad \}=\{7, \quad 8, \quad 9\} \quad (9)$$

where V_L is the field of sliding distance of earthquake landslide, and μ_H, μ_α , and μ_M are respectively the field of relative altitude, average gradient and volume. The predicting results by means of FIP are compared with those by other methods of SF, MF and EF shown in Fig.13.

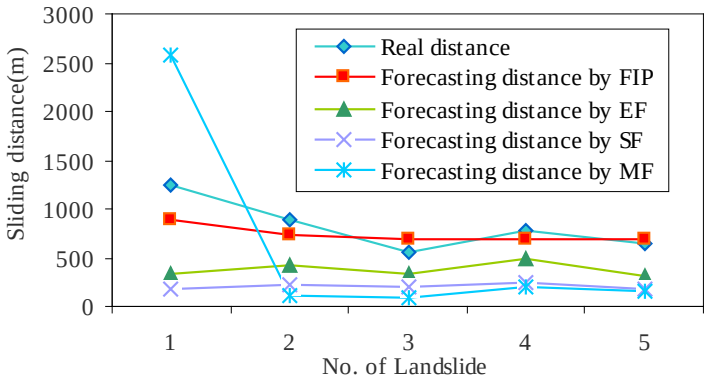

Fig.13 – Comparison in the sliding distances estimated by different forecasting methods

Fig.13 shows that the sliding distances of loess landslides estimated by the FIP method is closer to the real cases comparing than those by the other methods. In FIP model, consideration of intensity parameter makes the slip forcasting results more accurate, which also has been verified by error checking of actual sliding.

Most of the landslides affecting regions show a shape of horseshoe under the effect of earthquakes in loess areas. The area of affecting region can be calculated by integral of sliding distance L and estimating result of cross section width of landslide W shown in Fig. 14.

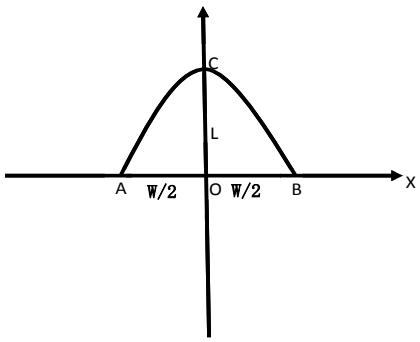

Fig.14 The area of landslide affecting region

The horseshoe shape area enclosed by parabola ABC and axis X can be got by the value of L and W. Then the coordinate of the three points A,B, and C can be known which are respectively (-W/2 0),(W/2 0) and (0 L), which can be used to calculate the formula of parabola ABC. At last, the integral area of the horseshoe shape area will be the estimated affecting region of loess earthquake landslide.

In spite of forecasting the influence region of loess earthquake landslide based on the above-mentioned fuzzy information processing method, the avoidance distances for buildings to preventing landslides disasters in loess area was provided, which has been adopted by Specification for Seismic Design Code of Buildings in Gansu Province. The avoidances are determined by both the affecting region of landslides and amplification region of seismic ground motion of a loess slope based on the field investigation and forecasting results. In the code, the avoidance distance from buildings to slope top edge should be longer than five times of slope height; the avoidance distance from buildings to slope toe should be longer than 1.5-2.5 times of slope height.

6. Conclusions

Water content has a predominant influence on both static strength and dynamic strength of loess. Static and dynamic internal friction angles will dramatically reduce with increasing of water content. Static and dynamic cohesions decrease obviously with increasing of water content.

Under the effect of a strong earthquake, fissures may develop in a loess slope, which will become the passes for raining water seepage. If the loess slope suffers continuous rainfall or heavy rainfall, a large scale landslide may occur due to predominantly decreasing of strength of the slope soil mass.

Under the effect of a middle-strong earthquake, small fissures may develop in a loess slope with gentle gradient, which have less influence on its stability. If the slope suffers light rainfall, it has a very low possibility of occurrence of landslides.

The stability of a loess slope will change a lot after suffering different rainfalls. For a loess slope with gentle gradient, the critical peak ground accelerations to induce its sliding failure are respectively 1g,0.7g and 0.6g in a natural condition, a light rainfall of 10mm and a heavy rainfall of 100mm.

The seismically failure mechanism of loess slopes is different in different rainfall conditions. For a natural loess slope with low water content, its seismic failure is caused by tension fractures in the middle and upper part of the slope. For a loess slope after suffering light rainfall, its seismic failure is induced by seismic subsidence. For a loess slope after suffering a continuous raining with long period or heavy rainfall, its seismic failure is caused by liquefaction induced mudflow.

The failure and its subsequent hazards of loess slopes under the coupling effects of earthquakes and rainfall may be predicted by the sequence and extent of the two factors. The methods of evaluating the sliding distance and affecting area of a loess landslide provided by the authors may be used for loess landslides hazard mitigation and prevention.

7. Acknowledgement

This paper is supported by the National Natural Science Foundation of China (No. 51478444). Mr. P. Wang, S. Chai, X. Zhong and K. Liu are appreciated for their assistance to the related tests in this paper.

8. References

[1] Aleotti P, Chowdhury R(1999): Landslide hazard assessment: summary review and new perspectives. Bulletin of Engineering Geology and the Environment, 58, 21-44.

[2] Hovius N, Stark C. P, Allen P. A(1997): Sediment flux from a mountain belt derived by landslide mapping. Geology, 25, 231-234.

[3] Schuster R. L(1996): Socioeconomic significance of landslides. In Turner, A. K, Schuster, R. L. (Ed.), Landslides, Investigation and Mitigation. Transportation Research Board Special Report, 247, National Academy Press, Washington, D. C., 12-36 .

[4] Garcia-Rodriguez, M. J., Malpica, J. A., Benito, B., Diaz, M.(2008): Susceptibility assessment of earthquake-triggered landslides in El Salvador using logistic regression. Geomorphology, 95, 172-191.

[5] Wang, L.M., Wu, Z.J.(2013): Earthquake Damage Characteristics of the Minxian-Zhangxian Ms6.6 Earthquake and Its Lessons. China Earthquake Engineering Journal, 35(3), 401-412.